Tunnelling and Underground Space Technology 52 (2016) 168–181

Contents lists available at ScienceDirect

Tunnelling and Underground Space Technology

journal homepage: www.elsevier.com/locate/tust

Influence of deep excavation induced ground movements on adjacent piles

D.S. Liyanapathirana *, R. Nishanthan

School of Computing, Engineering and Mathematics, Western Sydney University, Locked Bag 1797, Penrith, NSW 2751, Australia

ARTICLE INFO

Article history:
Received 20 November 2014
Received in revised form 28 October 2015
Accepted 24 November 2015
Available online 18 December 2015

Keywords:
Deep excavations
Ground movements
Wall support systems
Finite element method
Pile behaviour

ABSTRACT

In urban areas, excavations for cut-and-cover tunnels and basement construction cause detrimental effects on adjacent existing piles. Hence quantifying the excavation induced lateral deformations and bending moments on piles are important to ensure the stability of structures. In this paper, behaviour of a single pile subjected to excavation induced ground movements is analysed using the finite element method, which has the ability to simulate the construction sequence comprising soil excavation, deformations due to dewatering within the excavation and installation of struts. A fully coupled analysis is carried out based on the effective stress principle. The numerical model was verified using the centrifuge test data found in the literature. A parametric study was carried out to establish the excavation induced pile behaviour varying the depth of the excavation, soil properties, wall support system, pile fixity conditions and pile location with respect to the excavation. Increasing axial load does not have a significant influence on the pile behaviour. However, pile head fixity condition, and stiffness and spacing of the wall support system have a significant influence on the pile behaviour adjacent to the excavation. Finally, based on the parametric study, a set of design charts are developed to predict the pile behaviour by taking into account the depth of excavation, undrained shear strength, width of the pile, spring stiffness, spacing of vertical supports, and unsupported depth of the excavation. The capability of the proposed design charts are demonstrated using a three-dimensional finite element analysis, a case study from the literature and a previously published simplified analysis procedure.

1. Introduction

The need for urban construction involving deep excavations for basement construction and underground infrastructure such as mass rapid transit and cut and cover tunnels are increasing due to rapid urbanisation. Stress release caused by these deep excavations may lead to excessive lateral ground movements. The interaction of these lateral ground movements with nearby existing pile foundations develop additional loading on them. These additional loads will induce extra bending moments and lateral deformations on nearby existing pile foundations and they should be taken into account to ensure the integrity of the foundations as well as the structures supported by them.

Case studies with proper instrumentation (Finno et al., 1991; Goh et al., 2003) are very useful to gain a clear insight into the pile behaviour during nearby excavations. Also they can be used to verify numerical models. However, applying instrumentation along an existing pile shaft is not feasible prior to a nearby excavation. Hence the amount of data available is limited for existing pile behaviour during nearby deep excavations.

For problems similar to this, where it is not possible to instrument existing pile foundations, centrifuge tests play a major role. They can be used to investigate the pile behaviour and subsequently, measured response can be used to calibrate numerical models. Leung et al. (2000) and Ong et al. (2006) carried out centrifuge tests to investigate single pile response near excavations in sand and clay, respectively. Leung et al. (2000) found that the maximum induced bending moment and lateral deformation of the pile reduce exponentially with increasing distance from the excavation face and the provision of restraints at the pile head induce additional bending moments and shear forces. Ong et al. (2006) found that the wall and soil continue to move towards the excavation even after completion of the excavation due to the dissipation of excess pore water pressures. As a result, bending moment and pile lateral deformation increases with time even after the completion of the excavation. They identified a significant soil deformation zone, which is bounded by the wall and a line drawn from the bottom of the clay layer to the ground surface, 45° inclined to the wall. When the pile length within the significant

* Corresponding author.
E-mail address: s.liyanapathirana@westernsydney.edu.au (D.S. Liyanapathirana).

http://dx.doi.org/10.1016/j.tust.2015.11.019
0886-7798/

zone decreases (pile moves away from the wall), excavation induced pile response significantly decreases. Centrifuge tests discussed above did not consider the influence of axial loads applied on piles during nearby excavations. Guo and Ghee (2006) carried out scaled model tests in sand to investigate pile behaviour due to lateral ground movements incorporating axial loads supported by piles. They concluded that the axial load imposed on a pile head tends to decrease the induced bending moment, soil reaction and pile lateral deformation.

When performing parametric studies, numerical analyses are very cost effective compared to experimental modelling. The tools like finite element method can be used to simulate the construction sequence, wall support system, water drawdown, nonlinear soil behaviour, pore pressure effects and pile-soil interaction. In addition, actual geometry and three-dimensional nature of the problem can be taken into account. However, the three-dimensional finite element analyses require high computational effort and time. Therefore, in majority of finite element analyses, the analysis was carried out in two stages decoupling the ground response due to excavation and pile response. In the first step of these analyses, the free field movements are calculated using the finite element method or analytical solutions independent of the presence of the pile. In the second step, pile response will be computed by applying the computed free field movements to the soil adjacent to the pile, where soil–pile interaction is represented by a series of spring elements or p–y curves.

Poulos and Chen (1996, 1997) established design charts based on results from a two-stage analysis procedure. First they used a plane-strain finite element analysis to obtain ground deformations due to excavations. Then a pile analysis based on the boundary element method was carried out applying computed lateral soil movements as input. They investigated influence factors such as depth of excavation, stiffness and spacing of the support system, soil properties, pile head condition and pile diameter on maximum bending moment and maximum lateral deformation of a single pile adjacent to an excavation in undrained clay. Also they considered both unsupported and braced excavations. Xu and Poulos (2000) and Zhang et al. (2011) used a source-sink imaging technique proposed by Sagaseta (1987) to calculate the free-field soil movements. These calculated free-field movements are applied to soil adjacent to the pile, where soil–pile interaction is represented by a series of springs or p–y curves. They found that with an increase in working load acting over pile, the excavation induced pile settlement increases but the applied working load does not have much influence on the lateral response of the pile.

Poulos (2005) investigated the effect of excavations for a new pile cap adjacent to an axially loaded pile with different pressures over ground surface to simulate the loads applied by an existing building using the finite difference method. It was found that substantially higher lateral movements and bending moments are induced in the pile when the surface pressure is high. There is a higher chance for the induced moments to exceed the design capacity of the pile. Also he showed that the bending moments and shear forces due to induced lateral deformations are significant compared to those due to induced vertical deformations.

In this paper, a three-dimensional finite element analysis is carried out, which takes into account the coupling of ground movements due to excavations on pile response. The main aim of this paper is to investigate the pile behaviour due to lateral ground deformations caused by nearby excavations and to develop some design charts to predict pile behaviour. Hence soil anisotropy effects are not incorporated in this analysis owing to the large number of empirical parameters involved in those constitutive models, which might hinder the main purpose of this research. The shear modulus variation with strain level is incorporated in the parametric study carried out using the Modified Cam Clay (MCC) model. Prior to the parametric study, the model verification is carried out using centrifuge test results reported by Ong et al. (2006) for pile bending moments and lateral deformations. In the parametric study, pile behaviour is investigated during a nearby excavation by varying the spacing and stiffness of the wall support system, pile location, pile fixity conditions, over consolidation ratio of soil and axial load applied on the pile head. Based on the results from the parametric study, a set of design charts are developed considering the influence of depth of excavation, undrained shear strength, width of the pile, stiffness and spacing of struts supporting the wall, and unsupported depth of excavation on the pile response. Finally the design charts are validated using the results from a three-dimensional finite element analysis, case study from the literature (Finno et al., 1991) and a simplified method based on the design charts proposed by Poulos and Chen (1997).

2. Validation of three-dimensional finite element model using centrifuge data

The finite element model used in this analysis is verified using the centrifuge test results reported by Ong et al. (2006) to investigate whether the approaches used to model the wall, pile, and wall–soil and pile–soil interactions are appropriate to investigate the pile behaviour during an adjacent deep excavation.

2.1. Description of the centrifuge test

Centrifuge tests used for model validation were performed to investigate the behaviour of a single pile founded in clay, closer to an excavation behind an unsupported stable wall. Tests were carried out using the geotechnical centrifuge facility at the National University of Singapore at a centrifugal acceleration of 50g. The model container used for these tests has dimensions of 540 mm × 200 mm × 470 mm. The Malaysian kaolin clay was filled up to a depth of 130 mm above a Toyoura sand layer, which has a thickness of 120 mm. Fig. 1 shows the variation of undrained shear strength of the clay with depth obtained using a T-bar penetrometer test (Ong et al., 2006). The distribution shows that the top 2.5 m soil crust was over consolidated and soil below the crust was normally consolidated. The soil region that needs to be excavated was replaced by a Latex bag filled with a $ZnCl_2$ solution, which has a unit weight equivalent to clay. The excavation was

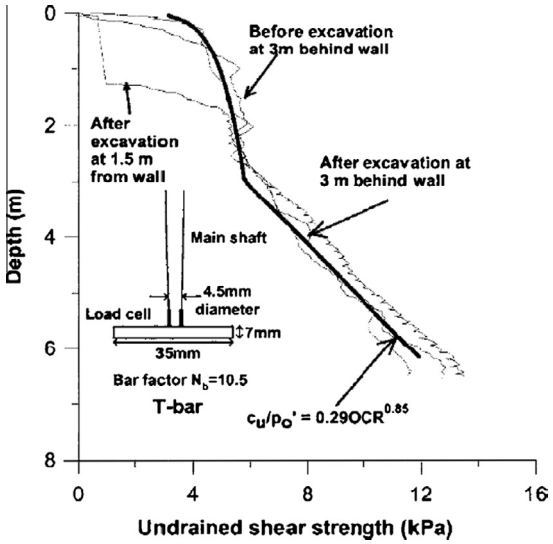

Fig. 1. Variation of undrained shear strength with depth (Ong et al., 2006).

carried out during the centrifuge test by draining the $ZnCl_2$ solution at 50g in six stages over two days.

2.2. Material models and properties

The finite element analysis simulating the centrifuge test was carried out using the ABAQUS/Standard (2011) finite element program. The stress–strain behaviour of the Malaysian kaolin clay used for the centrifuge test was simulated using the Modified Cam Clay (MCC) model. Constitutive models with linear elasticity is not suitable to predict the ground surface settlements or pile settlements during excavations due to ground heave predicted near the wall (Potts and Zdravkovic, 2001). Therefore, in this case shear modulus, G, of the soil is varied with the void ratio, e, as shown below:

$$G = \frac{3(1-2\nu)}{2(1+\nu)}\frac{(1+e)p'}{\kappa} \quad (1)$$

where p' is the mean effective stress, κ is the slope of the swelling line and e depends on strains. Above equation introduces a nonlinear shear modulus to the analysis, without introducing any additional model parameters to the soil constitutive model.

The material properties for the Malaysian kaolin clay were assigned based on the properties given by Ong et al. (2006) and Teh et al. (2005). The compression index and swelling index of the clay are 0.64 and 0.14 respectively. These values correspond to a gradient of virgin consolidation line, λ, of 0.244 and a gradient of swelling line, κ, of 0.053 in the $e-\ln(p')$ space. Poisson's ratio for the clay was assumed as 0.3. Lateral earth pressure coefficient at rest, K_o, for the clay is 0.6 and the unit weight of the soil is 15.21 kN/m^3 (Ong et al., 2006). According to Teh et al. (2005), the slope of the critical state line in the $p'-q$ space, M, is 0.9, permeability, k, is 1.36×10^{-8} m/s and void ratio of the virgin consolidation line in the $e - \ln(p')$ space at the unit pressure, e_1, is 2.35.

The Toyura sand layer below the clay layer was modelled using the Mohr–Coulomb model considering the consolidation behaviour with an internal friction angle of 43°, dilation angle of 15°, permeability of 1.36×10^{-7} m/s, an effective cohesion of zero and a Young's modulus of 6z MPa, where z is the depth below the ground surface in metres (Ong et al., 2006). The Poisson's ratio of the sand is assumed to be 0.3.

The pile used in the centrifuge model was a hollow square aluminium tube and in prototype scale bending stiffness of the pile is 2.2×10^5 kN m^2, which is equivalent to a 600 mm diameter concrete pile with an embedment depth of 12.5 m. The wall used in the centrifuge test was a 3 mm thick aluminium plate, with prototype bending stiffness of 24×10^3 kN m^2/m, which is equivalent to a steel sheet pile wall with an embedment depth of 8 m. Both pile and wall were modelled assuming linear elastic behaviour. Fig. 2 shows the cross-section of the excavation profile used for the centrifuge test.

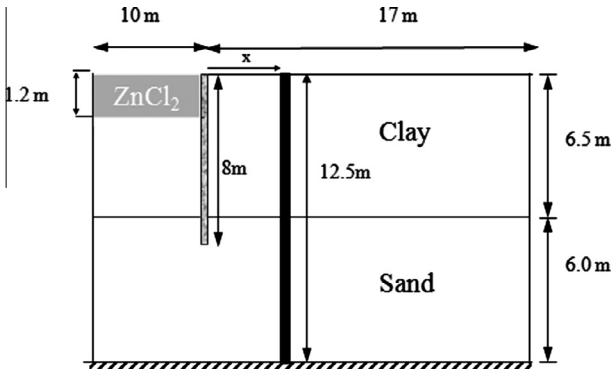

Fig. 2. Cross section of the centrifuge model with excavation.

2.3. Finite element modelling

The centrifuge test was modelled using a three-dimensional finite element model created based on the prototype dimensions of the problem as outlined in the previous section. Only half of the problem was modelled due to the symmetry of loading and geometry. Fig. 3 shows the plan and side view of the finite element mesh used for the analysis.

Pile, wall and soil were modelled using twenty-node quadrilateral brick elements with a reduced integration formulation. The structured meshing technique was used to mesh the wall, pile and the soil. Swept meshing was used for the soil region near the pile. The bottom soil nodes were restrained from movement in all directions ($u_x = u_y = u_z = 0$). Since grease was applied along all four vertical sides of the container, nodes over these side faces are free to move in the vertical and horizontal directions along the side faces of the container. Hence four vertical sides of the finite element mesh are restrained only in the directions perpendicular to the side faces. A pinned boundary condition was used at the bottom of the pile, which was in touch with the base of the container used for the centrifuge test. Since solid elements were used for the pile, restraining the movement in all directions at the pile toe will create a fixed boundary condition resulting a high bending moment at the toe of the pile. To avoid this problem, only the bottom centre node of the pile tip was restrained in the horizontal and the vertical directions simulating a pinned node.

Surface to surface contact modelling technique in ABAQUS/Standard (2011) was used to simulate the pile–soil and wall–soil interfaces. Coulomb friction model was used to simulate the soil–pile and wall–soil interactions, which is governed by a friction coefficient and a limiting displacement for elastic slip. Shear stress which can develop at the pile–soil interface is limited when it reaches the friction coefficient times the normal stress at the interface. Analyses carried out with different coefficients of friction show that the behaviour of laterally loaded pile is not significantly affected by the soil–pile interface friction coefficient, if slippage and separation are allowed at the interface. This observation agrees with the comments made by Brown and Shie (1990). Here a value of 0.3 was selected as the friction coefficient. A limiting displacement of 5 mm was selected for the elastic slip to mobilise the full skin friction at the pile–soil interface based on the typical values

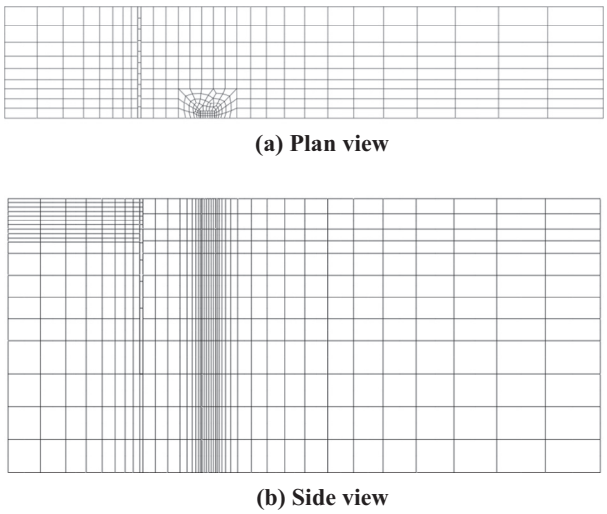

Fig. 3. Plan and side views of the finite element mesh used for the analysis.

reported by Broms (1979). Another advantage of allowing slippage and separation at the pile–soil interface is that it will avoid the overestimation of the bending moment of the pile as well as the soil pressure exerted on the pile (Miao et al., 2006). Excavation was simulated by removing the elements up to a depth of 1.2 m. Bending moments developed in the solid continuum pile is extracted as a section output of the pile as described in ABAQUS/Standard (2011), which is calculated based on the internal stresses acting over the elements within the defined section.

In ABAQUS/Standard (2011), consolidation analysis can be carried considering total pore pressures or excess pore pressures. When modelling excavations below the water table using the finite element method, it is important to define pore pressures in terms of total values, which takes into account the hydrostatic pore pressures acting on the wall. If excess pore pressures were considered in the analysis, hydrostatic stresses need to be applied to the wall from the retained soil as separate body loads considering the water level within the excavation and retained soil behind the wall due to dewatering (Nishanthan et al., 2014). In the current analysis, the initial geostatic stress state is established applying the initial unit weights of materials to the finite element model using the GRAVITY option in the finite element program to carry out the analysis in terms of total pore pressures. The non-uniform initial void ratio distribution within the soil is defined using the user defined subroutine VOIDRI and the dry density of the soil calculated using the void ratio and specific gravity of 2.65 was used for the material density (ABAQUS/Standard, 2011). The 1.2 m deep excavation was carried out during 2.2 days simulating the same rate of excavation as described by Ong et al. (2006).

2.4. Comparison of results

Fig. 4(a) and (b) shows the measured and predicted pile lateral deformations and bending moments at the end of excavation depth of 1.2 m. The predicted pile lateral deformation and bending moment agree well with the measured values. Since the wall is unsupported during the excavation, cantilever type deformation was observed throughout the excavation.

During the centrifuge tests, bending moments were obtained using calibrated strain gauges. Then the lateral deformation profile was obtained by double integrating the bending moment profile considering the boundary conditions at the pile tip and pile head. Since there is no rotational restraint at the top and bottom surfaces of pile, zero bending moments were obtained from the centrifuge test and the finite element analysis. In the finite element analysis, bending moments were extracted by defining sections along the pile. Overall, these results show that the finite element model with Coulomb frictional contact at the wall–soil and pile–soil interfaces, elastic behaviour assumed for the pile and wall, MCC model applied for the Malaysian kaoline clay and the total pore pressure option used for the simulation of the centrifuge test has the ability to predict the pile behaviour with reasonable accuracy. Therefore a similar finite element model with material properties, boundary conditions and interaction properties is adopted for the parametric study outlined in the following section.

3. Parametric study

3.1. Scope of the study

This study focuses on the response of a single pile, where the pile is located behind an excavation. During the parametric study, excavation depth, pile location with respect to the wall, spacing between struts used to support the wall, stiffness of the struts, unsupported depth of the excavation, pile width, over consolidation ratio (OCR) of the soil and pile head fixity are varied while keeping the same geometry of the excavation. Parametric study is conducted using a three-dimensional finite element model and the cross section of the three-dimensional problem analysed is shown in Fig. 5. The numerical results presented in the parametric study correspond to the values at the end of each excavation stage.

The excavation is supported by a 40 m long and 1 m thick diaphragm wall. The square single pile is 50 m long and the side width is 1 m. The wall and the pile are made of concrete, which has a Young's modulus of 40 GPa. The floating pile does not have any restraints at both ends. The soil domain was extended five times the width of the square pile measured from the centre of the pile in the horizontal transverse direction, which is the direction perpendicular to the side view shown in Fig. 5. In the vertical direction, soil domain extends a distance equivalent to the wall

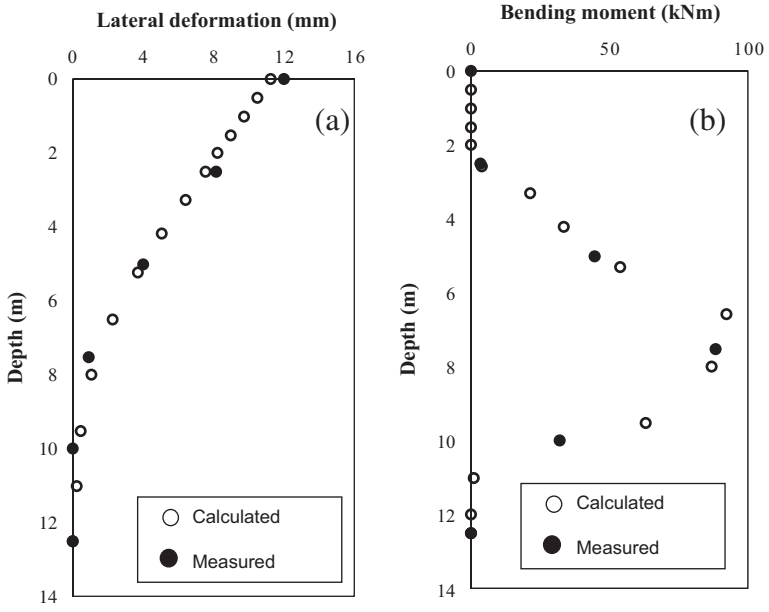

Fig. 4. (a) Pile lateral deformation and (b) bending moment along pile shaft at the end of the excavation.

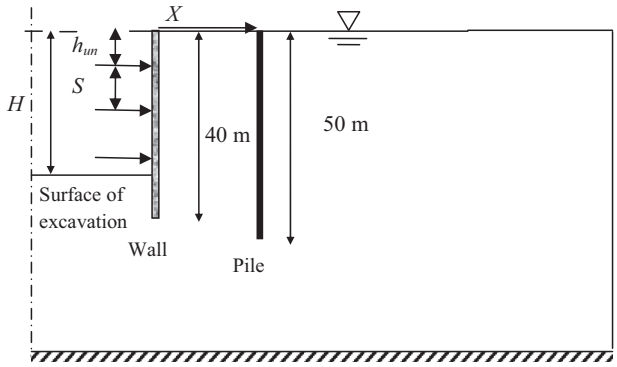

Fig. 5. Geometry of the excavation (side view) used in the analysis.

length, measured from the bottom of the wall. In the longitudinal direction (X direction marked in Fig. 5), the soil domain extends five times the wall length, measured from the centre of the excavation. These boundaries were selected simulating a number of cases with different mesh sizes. Since these boundaries are placed far away from the pile, they will avoid boundary effects on the pile response. The analysis neglects installation effects of the wall on existing pile and concentrates only on the pile behaviour due to excavation induced ground deformations.

The bracing system used to support the wall is idealized using single-node spring elements. A simple construction sequence is used in the analysis as shown in Fig. 5. Soil elements were removed up to a depth of h_{un} and the first strut is installed at the level of the newly excavated surface. Then the excavation proceeds up to a depth of $(h_{un} + S)$ and the second strut is installed at this level, where S is the distance between struts. Inside the excavation the water table is maintained 2 m below the newly excavated surface to simulate the lowering of water table due to pumping inside the excavation. Also this helps to overcome convergence problems associated with finite element modelling of excavations. For the soil behind the excavation, water table is kept at the ground surface.

The material properties used for the clayey soil are shown in Table 1. The clay has a gradient of virgin consolidation line, λ, of 0.17 and a gradient of swelling line, κ, of 0.034 in the $e-\ln(p')$ space, Poisson's ratio of 0.3, lateral earth pressure coefficient at rest, K_o, of 0.53 and unit weight of 18 kN/m^3. The slope of the critical state line in the $p'-q$ space, M, for the normally consolidated clay is 1.1 and the permeability, k, is 1.0×10^{-5} m/day. Table 2 shows the variation of geometric parameters for the cases analysed. Fig. 6 shows the soil flow around the wall and pile, which is 3 m behind the wall, when the excavation depth is 28 m. This figure clearly shows that the nonlinear stiffness used for the analysis has avoided the heave behind the wall, which is a significant problem when linear elastic soil models are adopted in finite element simulations as explained by Potts and Zdravkovic (2001). In Fig. 6 there is a slight upward heave behind the wall, but the ground surface predominantly moves in the lateral direction towards the excavation. This slight heave is due to soil movement beneath the excavated surface. Stress release due to excavation causes a heave over the excavated surface. As a result, soil around the tip of the pile and wall flows towards the excavation in the horizontal direction and vertically in the upward direction towards the surface of the excavation causing a small heave behind the wall.

Table 1
Soil parameters used in the analysis.

Soil parameters	Symbol	Value
Unit weight (kN/m^3)	γ	18.0
Void ratio	e	1.0
Poisson's ratio	ν	0.3
Stress ratio	M	1.1
Log plastic bulk modulus	λ	0.17
Log elastic bulk modulus	κ	0.034
Lateral earth pressure coefficient	K_0	0.53
Permeability (m/day)	$k_x \cdot k_y$	1.0×10^{-5}

Table 2
Material and geometric properties used for the parametric study.

Parameters	
Depth of excavation (H)	4, 8, 12, 16, 20, 24, 28 m
Unsupported depth (h_{un})	0, 2, 4, 6 m
Spacing (S)	2, 4, 6, 10 m
Location (X)	1, 3, 5, 10, 15, 25, 40, 60, 100 m
Over Consolidation Ratio (OCR)	1, 2, 4
Pile head fixity	Free/pinned/fixed
Spring stiffness	1, 10, 50, 100, 200, 500, 1000 MN/m/m
Axial load	1, 2, 4, 8, 16 MN

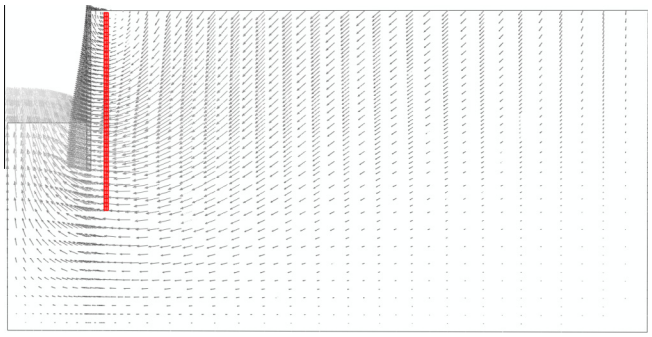

Fig. 6. Soil flow around the pile and wall at excavation depth of 28 m.

4. Analysis of results

4.1. Effect of excavation depth

Fig. 7 shows the variation of excavation induced pile movement in the lateral direction and bending moment during different stages of the excavation. For the results given in Fig. 7, the pile is located 3 m away from the wall, which is supported by struts having a vertical spacing of 2 m. The first row of struts with a stiffness of 200 MN/m/m was assumed to be fixed at the surface level. According to Fig. 7(a), the maximum induced lateral deformation increases linearly with the excavation depth and deformation is about 1.0% of the excavation depth, H. The maximum lateral deformation of the pile occurs well below the excavation depth and during the excavation, there is a shift at the pile toe, which is about 40% of the maximum pile lateral deformation when H is 4 m and it gradually increases to 70% of the maximum pile lateral deformation when H is 28 m. Even though the first strut is installed at the surface level before excavating the first 2 m depth, the pile has a slight lateral deformation at the top during the initial stages of the excavation and it rebounds to the original position due to the installation of subsequent struts and the pile rigidity.

Fig. 7(b) shows the progression of the bending moment along the pile shaft during the excavation. Maximum bending moment values are increasing approximately linearly with the depth of excavation. For the results presented in Fig. 7(b), maximum bending moment developed is about $140H$ kN m, where H is in metres. When the excavation depth is shallower, the maximum curvature of the bending moment profile is observed in the upper part of the

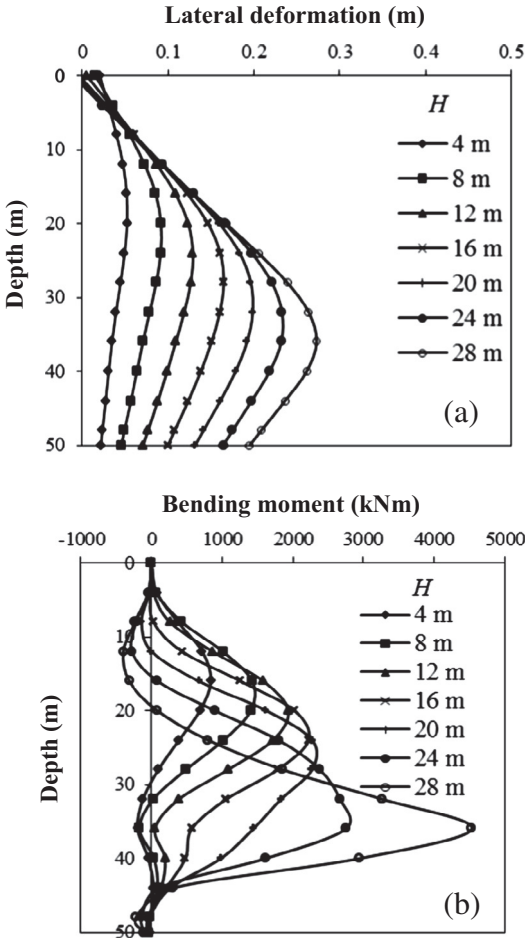

Fig. 7. Effect of depth of excavation on (a) pile lateral deformation and (b) bending moment (X = 3 m).

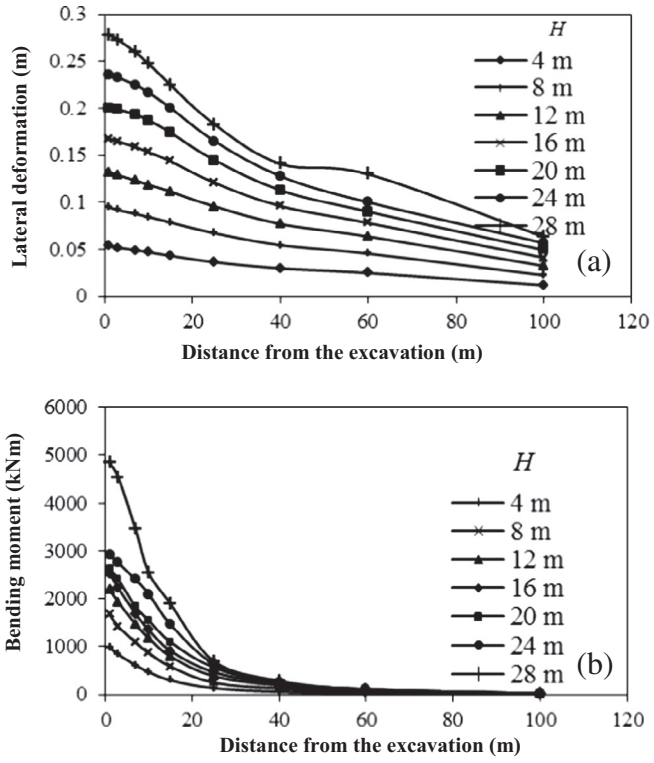

Fig. 8. Effect of pile location on (a) pile lateral deformation and (b) bending moment.

pile. As the excavation depth increases, the upper part tends to bend in the opposite direction due to the support provided by the struts and the maximum bending moment occurs where the pile have maximum lateral deformation.

4.2. Effect of pile location

Fig. 8(a) and (b) shows the variation of pile lateral deformation and bending moment, respectively, with the pile location at various stages of the excavation. For any particular excavation depth, both the maximum lateral deformation and maximum bending moment decreases exponentially with the distance away from the excavation as shown below.

$$d_{max} = \frac{H}{100} e^{-0.015x} \text{ m} \quad (2)$$

$$M_{max} = 140He^{-0.05x} \text{ kN m} \quad (3)$$

where x is the distance measured away from the excavation and H is the excavation depth, in metres. For any particular pile location, maximum lateral deformation and maximum bending moment varies linearly with excavation depth. The maximum bending moment, which is obtained when the pile is located as close as 1 m from the wall, diminishes to a value less than 10% of that value, at a distance of 50 m away from the excavation regardless of the depth of the excavation. The maximum lateral deformation, which is obtained when the pile is located as close as 1 m from the wall, diminishes to about 50% of that value at a distance of 50 m away from the excavation, regardless of the excavation depth. The rapid reduction in pile bending moment compared to the reduction in pile lateral deformation, when moving away from the excavation, indicates that the pile is subjected to shifting rather than bending when moving away from the excavation.

4.3. Effect of support system

Fig. 9(a) and (b) shows the influence of support spacing on pile lateral deformation and bending moment, respectively. These results are for a pile located 3 m away from a 20 m deep excavation. When the vertical spacing of struts increases from 2 to 6 m, the amount of increment in lateral deformation (7%) and bending moment (13%) are not significant. When the struts are closely spaced, the maximum pile lateral deformation occurs well below the base of the excavation. However, for the minimal support case with 10 m strut spacing, the maximum lateral deformation can be observed near the excavation depth. Similar trend of lateral deformation profile for a wall supporting an excavation was observed by Hashash and Whittle (1996).

Fig. 10(a) and (b) shows the effect of stiffness of the wall support system on the lateral deformation and bending moment of the pile, respectively. The excavation is associated with an unsupported wall length of 0 m because the first strut was installed and then the first 2 m of soil was excavated. For the results shown in Fig. 10, struts are placed at 2 m interval along the wall. Pile bending moment and lateral deformation decreases significantly when the stiffness of the support system increases from 1 to 50 MN/m/m. However, when the stiffness of the support system is greater than 10 MN/m/m, the stiffness of the support system does not have a significant influence on the pile behaviour.

The effect of unsupported depth of excavation on pile lateral deformation and bending moment was investigated for two different stages of the excavation (depths of 8 m and 20 m) in normally

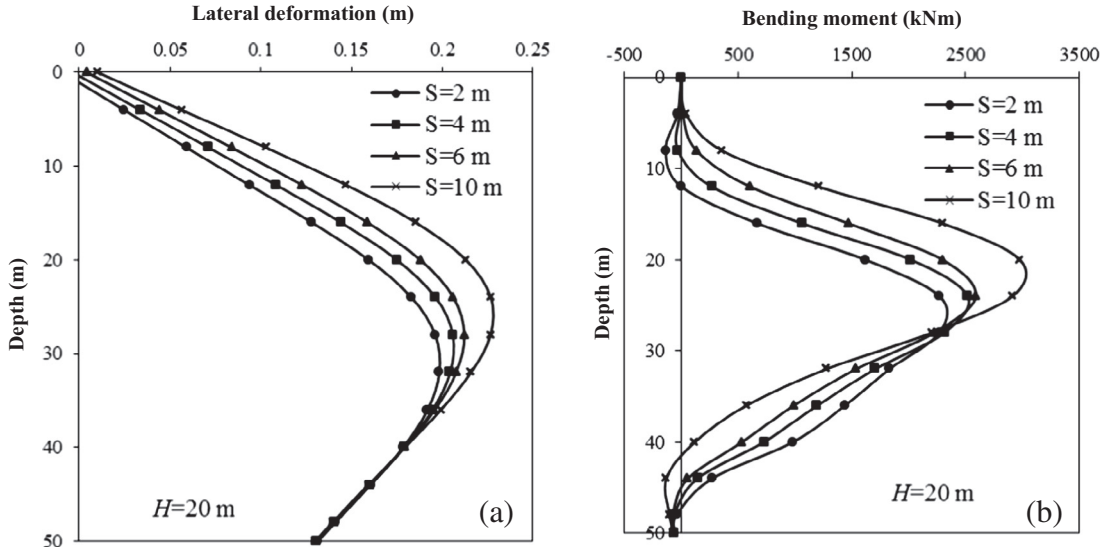

Fig. 9. Effect of vertical spacing of support system on (a) pile lateral deformation and (b) bending moment.

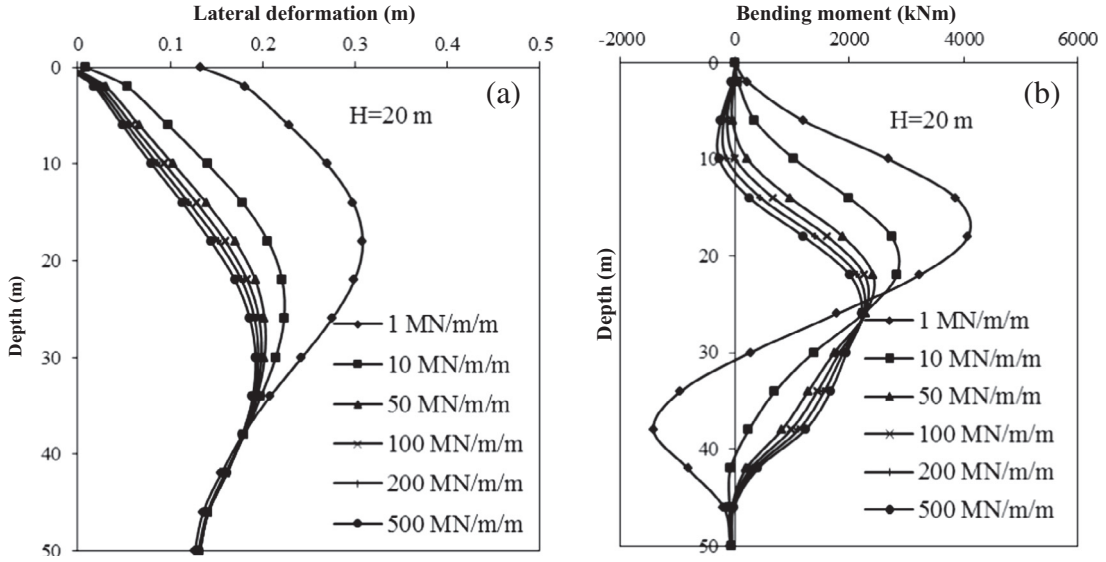

Fig. 10. Effect of spring stiffness on (a) pile lateral deformation and (b) bending moment.

consolidated clay as shown in Fig. 11(a) and (b). Even though the unbraced depth does not have much influence on the maximum lateral deformation of the pile, it has a significant influence on the lateral deformation profile of the pile closer to the pile head as shown in Fig. 11(a). Before the installation of the initial strut, the wall and soil behind it experience higher lateral deformations near the surface level. Since the pile head is located 3 m away from the excavation and free to move, cantilever deformation occurs at the end of the first strut installation. Further increase in curvature of the pile occurs with the installation of subsequent struts. A similar pattern of wall movements was observed by Hashash and Whittle (1996), and O'Rouke (1981) during deep excavations.

Fig. 11(b) shows the variation of bending moment. When the excavation depth is 8 m, with an unsupported depth of 6 m, less bending moment values were observed than those obtained with lower unsupported depths (h_{un} = 0, 2 and 4 m). This happens due to increased flexibility of the wall due to less support. Although pile stiffness does not change with support spacing or stiffness, pile bending moments are decreased with increasing support spacing in agreement with wall behaviour. There was a 40% reduction in maximum bending moment, when the unsupported depth of the excavation was increased from 0 to 6 m for the H = 20 m case.

4.4. Influence of soil stress history

The stress history of the soil significantly affects the deformation characteristics of the soil and subsequently the deformation characteristics of structures supported by them. Since the MCC model was used to model the constitutive behaviour of soil, OCR was used to change the initial pre-consolidation pressure and the lateral earth pressure coefficient, K_o, of the soil. In this case pile is located 3 m away from the wall, which is supported by struts having a vertical spacing of 2 m. The first row of struts with a stiffness of 200 MN/m/m was fixed at the surface level. Fig. 12(a) and (b) shows the effect of OCR on the pile lateral deformation and bending moment, respectively. Uniform OCR values of 1, 2 and 4 were considered throughout the depth. As expected, for over consolidated soils with high OCR values, the predicted pile lateral deformations are low and

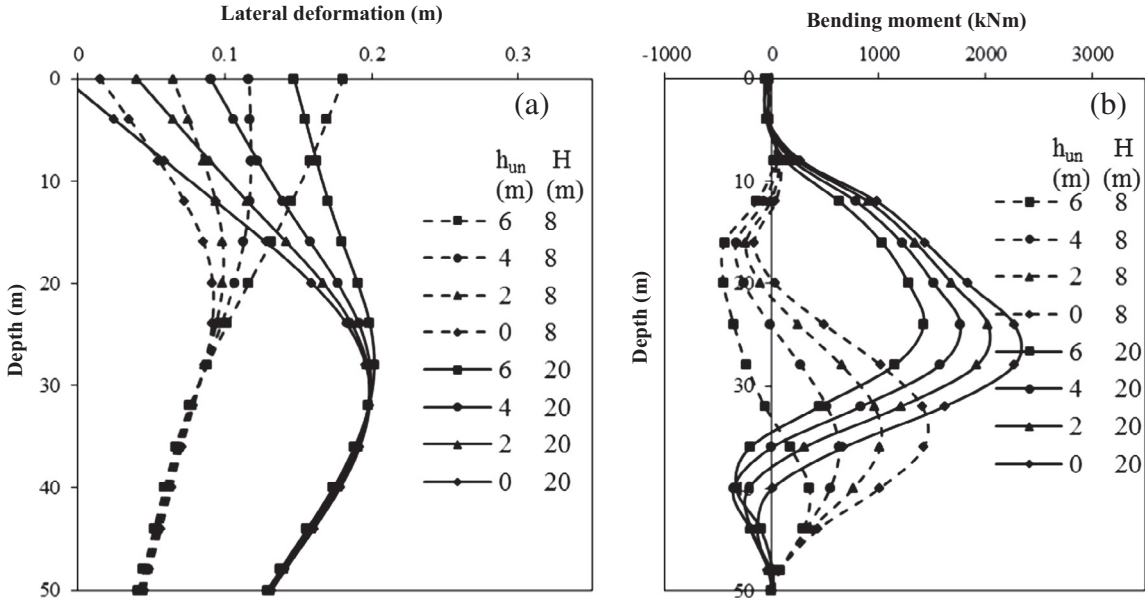

Fig. 11. Effect of unsupported depth of excavation on (a) pile lateral deformation and (b) bending moment.

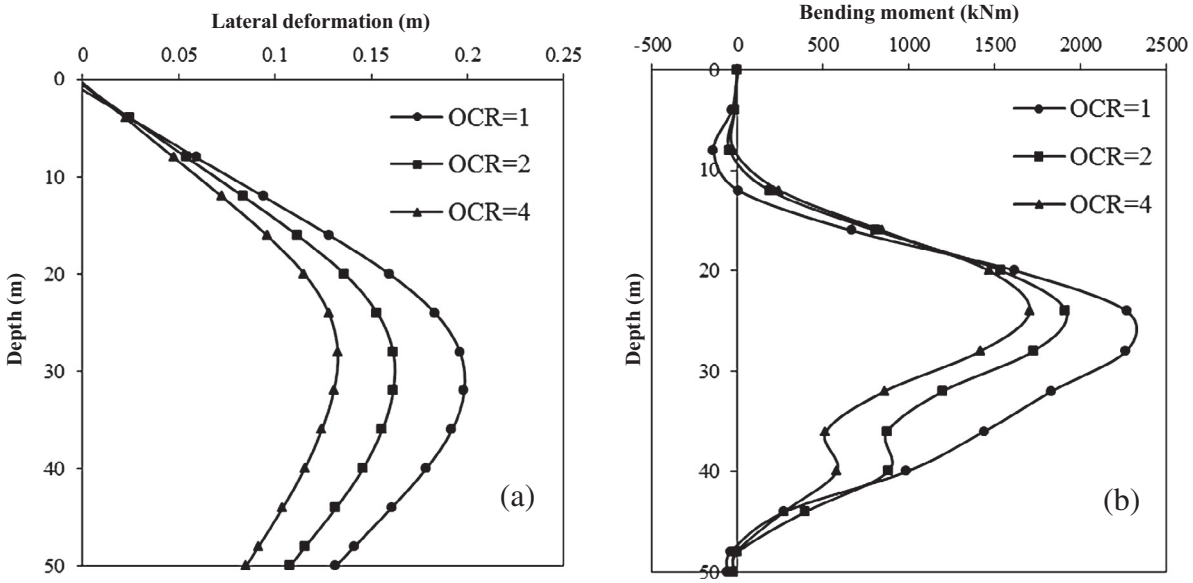

Fig. 12. Effect of OCR on (a) pile lateral deformation and (b) bending moment.

hence bending moments as well. When the OCR changes from one to four, pile lateral deformation was decreased by about 30% and pile bending moment is decreased by about 25%.

4.5. Influence of pile head fixity

Both centrifuge tests and numerical analyses show that the pile head fixity condition has a significant impact on the lateral pile response, when the pile is located adjacent to an excavation (e.g., Poulos and Chen, 1996; Leung et al., 2000). Therefore, the effect of pile head condition is investigated in the current analysis through three different boundary conditions at the pile head: (i) both translation and rotation free, (ii) translation fixed and rotation free (pinned) and (iii) both translation and rotation fixed. In the finite element model, Case (i) is simulated by a free head pile without applying any boundary condition at the pile head. Case (ii) is simulated by fixing only the centre node of the pile head. In Case (iii), all nodes over the pile head are fixed. Pile head condition with free translation and fixed rotation has not been considered here because it is not possible to simulate this boundary condition, when solid continuum elements are used to represent the pile.

Fig. 13 shows the pile response at the end of 4 m and 20 m depths of excavation for the case with unsupported excavation depth of 6 m. For this case, the pile is 3 m away from the excavation. It can be clearly seen that greater the pile head fixity, higher are the bending moments developed in the upper part of the pile. Due to the nature of the problem considered, high negative pile head bending moments of 8.5 MN m and 13.0 MN m were obtained for Case (iii) with the highest fixity condition at the end of 4 m and 20 m excavation depths, respectively. These maximum negative moments vary from about 3 to 4 times the maximum positive moments when the excavation depth increases from 4 m to 20 m.

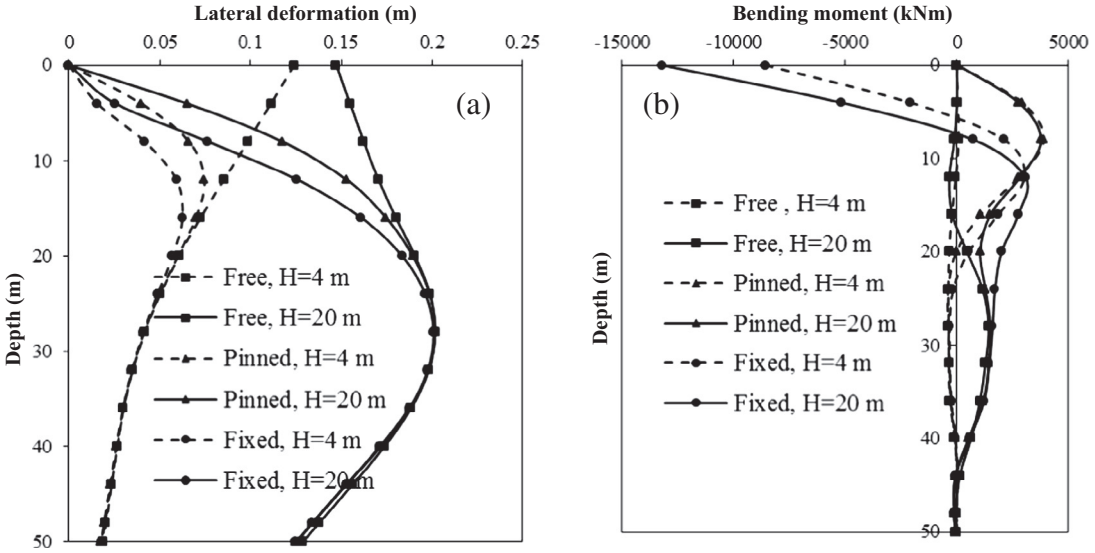

Fig. 13. Effect of pile head fixity on (a) pile lateral deformation and (b) bending moment.

Normally in practice, piles are tied using either a pile cap or tie-beams and finally connected to the superstructure. Therefore, pile head connections are normally partially fixed, in between Cases (ii) and (iii), depending on the pile head embedment into the pile cap and amount of reinforcements extending into the cap. For all three cases, the maximum positive bending moments does not have much difference as mentioned by Chen and Poulos (1996) and Leung et al. (2000).

Leung et al. (2000) investigated the effect of pile head fixity condition on pile response using centrifuge tests, where the pile is located 3 m behind an unbraced excavation. For the fixed pile head condition (both rotation and lateral deformation restrained), the negative moment observed near the top of the pile was slightly less than the maximum positive bending moment observed at the end of 4 m depth of excavation with an unsupported wall similar to the centrifuge test. The reason may be the method they used to create a fixed condition at the pile head. They used a clamp to make both pile lateral deformation and rotation zero at the pile head. If the clamp has not restrained the rotation at the pile head completely, bending moment developed at the pile head will be less than that developed under zero rotation simulated in the finite element model.

The deformation values for pile with fixed translation condition at the head are similar to those for the pile with free boundary condition at the head, when the excavation was braced at the surface level. The reason for this similarity is due to the strut at the ground level, which restraints the movement of wall and soil behind the wall towards the excavation.

4.6. Influence of axial load

For this case, the pile is 3 m away from the excavation, which is supported by springs with stiffness of 200 MN/m/m at 2 m spacing. The first level of struts was placed at the ground level. In this case the initial stresses in ground were obtained prior to application of the axial load. The induced lateral deformation and bending moment are not influenced by the axial load. The same observation was made by Zhang et al. (2011).

Fig. 14 shows the combined bending and axial load capacity envelope considering the ultimate and serviceability design strengths computed for reinforced concrete combining strengths of concrete and steel (Park and Paulay, 1975). According to this figure, when the bending moment increases, axial load carrying capacity of the pile decreases. According to the finite element results obtained in this study, when axial loads increased from 8000 kN to 16,000 kN, the increase in induced pile lateral deformation and bending moment are negligible. However, the bending moment carrying capacity of the pile reduces drastically when axial load increases from 8000 kN to 16,000 kN as depicted in Fig. 14. Conversely, with increasing bending moments, axial load carrying capacity of the pile decreases. Therefore, when an excavation is planned to be carried out near existing loaded pile foundations, it is important to assess how the bending moments induced due to excavation will affect the structural capacity of the pile foundation.

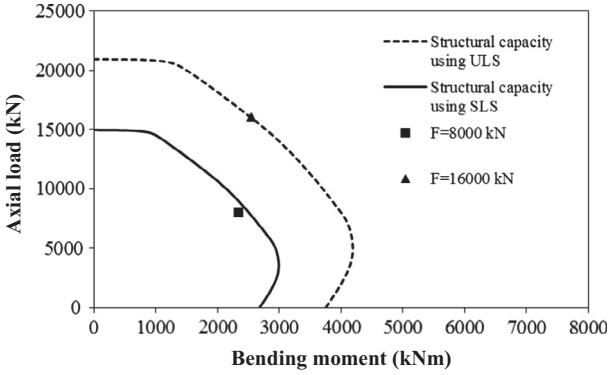

Fig. 14. Pile strength envelopes.

5. Design charts

The results obtained from the parametric study are unified to dimensionless quantities useful for practicing geotechnical engineers to assess behaviour of existing piles due to nearby excavations. Even though the numerical modelling was carried out using the MCC model, the design charts are presented using the undrained shear strength, which is commonly used as a geotechnical design parameter. Undrained shear strength for the soil is calculated using the MCC parameters using the following equation (Wroth and Houlsby, 1985):

$$\frac{c_u}{p'_c} = \frac{M}{2}\left(\frac{\mathrm{OCR}}{2}\right)^{\Lambda} \tag{4}$$

where $\Lambda = \frac{\lambda-\kappa}{\lambda}$, p'_c is the initial preconsolidation pressure, M is the slope of the critical state line in $p'-q$ space and λ is the slope of the normal consolidation line in the $e-\ln(p')$ space. The initial value of p'_c is computed using the initial effective stresses and the OCR. When developing the design charts for the base case, soil properties given in Table 1 were adopted. The pile used has a square section with 1 m width and it is located X m away from the wall, which is supported by struts having a vertical spacing of 2 m. The first row of struts with a stiffness of 200 MN/m/m was assumed to be fixed at the surface level.

The maximum induced pile lateral deformation and bending moment for any case can be approximated by Eqs. 5(a) and 5(b), which are based on the maximum lateral deformation and bending moment for the base case and a set of influence factors, similar to the method proposed by Poulos and Chen (1997):

$$d_{\max} = d_b \cdot k'_{c_u} \cdot k'_d \cdot k'_S \cdot k'_k \cdot k'_{h_{un}} \tag{5a}$$

$$M_{\max} = M_b \cdot k_{c_u} \cdot k_d \cdot k_S \cdot k_k \cdot k_{h_{un}} \tag{5b}$$

where $d_{\max}$ is the maximum lateral deformation, d_b is the maximum lateral deformation for the base case, $M_{\max}$ is the maximum bending moment, M_b is the maximum bending moment for the base case, k'_{c_u}, k_{c_u} are the influence factors for the undrained shear strength, k'_d, k_d are the influence factors for pile width, k'_S, k_S are the influence factors for vertical spacing, k'_k, k_k are the influence factors for spring stiffness and $k'_{h_{un}}$, $k_{h_{un}}$ are the influence factors for unsupported depth of excavation. The values for d_b and M_b for the base case can be computed using Eqs. (2) and (3) or Fig. 8 (a) and (b), respectively.

Figs. 15–19 show influence factors for different undrained shear strengths, pile sizes, spacing of struts, stiffness of struts and unsupported depths. Influence factors for each parameter variation are obtained by dividing the pile lateral deformation and bending moment for each case with the corresponding values for the base case. Hence each influence factor is one, when it is corresponding to the base case.

Fig. 15(a) and (b) shows the variation of k'_{cu} and k_{cu} with undrained shear strength of soil. Since we used the MCC model, change in undrained shear strength is achieved using Eq. (4). With increasing c_u, both correction factors decrease due to decrease in ground deformations due to increased shear strength of the soil. Although the observed trend in Fig. 15 is acceptable, it differs from the variation given by Poulos and Chen (1997), where the pile deformation increase with increasing undrained shear strength. Again in this case, variation of k'_{cu} with pile location is not significant. Influence factor, k_{cu}, for bending moment changes with pile location. When the pile is located 25 m $\leqslant X <$ 40 m, influence factors can be obtained by interpolating between the two curves given in Fig. 15(b).

The influence of width of pile on pile lateral deformation and bending moment are shown in Fig. 16(a) and (b). Influence factor for pile lateral deformation slightly decreases from 1 to 0.94 with increasing pile width from 1 to 2 m. When the pile is located 25 m or more away from the excavation, the pile width does not have any impact on the lateral deformation. Pile bending moment increases with increasing pile width due to increased bending stiffness. However, the pile bending moment is not affected by the pile location as shown in Fig. 16(b).

Fig. 17(a) and (b) shows the influence of support or strut spacing on the influence factors k'_s and k_s. When the pile location is within 10 m of the excavation, stiffer support system, which has the least vertical spacing, gives lower pile lateral deformations and bending moments due to less movement of wall and subsequently ground. With increasing distance between wall and pile, variation of influence factor, k'_s, is not significant. However, the influence factor, k_s, changes significantly. When the pile is closer to the excavation ($X \leqslant 10$ m), reduced strut spacing increases the influence factor for moment due to increase in curvature of the deformed pile. When the pile is some distance away from the wall ($X \geqslant 25$ m), pile deformation due to shifting is increased with strut spacing. Hence the influence factor k_s decreases with increasing spacing, due to reduced bending moment. The influence factors k'_k and k_k for strut stiffness are shown in Fig. 18. The trend shown for increasing strut stiffness is similar to decreasing strut spacing because both will have the same effect on ground and wall movements and subsequently on pile behaviour.

Fig. 19 shows that effect of unsupported depth of excavation on influence factors $k'_{h_{un}}$ and $k_{h_{un}}$. Larger unsupported depth increases ground deformations and hence the pile lateral deformations. However, bending moments are reduced with increasing unsupported depth of excavation due to reduction in curvature of the pile as shown in Fig. 11.

5.1. Validation of the proposed design procedure using the three-dimensional finite element model results

A problem with following properties was considered for the validation of the proposed set of design charts. The pile considered for this problem has a diameter of 1.5 m and located 25 m away from the proposed excavation. The soil profile has an OCR of 2, λ of 0.2, κ of 0.03, M of 1.1 and the strut system used to support the wall has a stiffness of 100 MN/m/m. The distance between struts is 4 m and the unsupported depth of the excavation is 2 m. The maximum

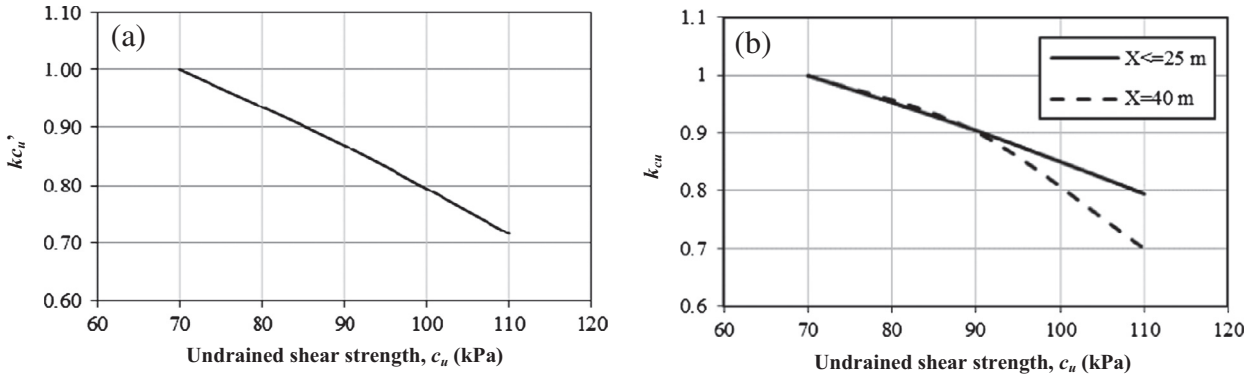

Fig. 15. Influence factors for undrained shear strength corresponding to (a) deflection and (b) bending moment.

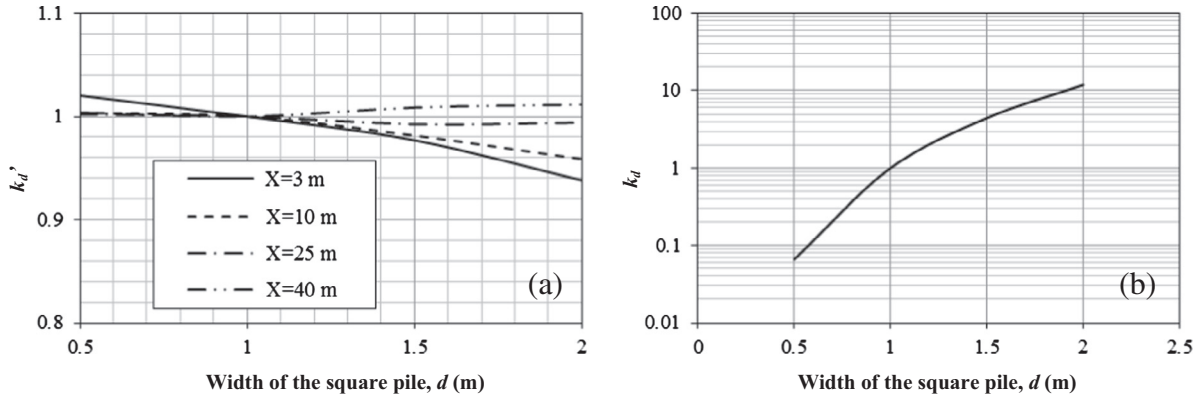

Fig. 16. Influence factors for width of the square pile corresponding to (a) deflection and (b) bending moment.

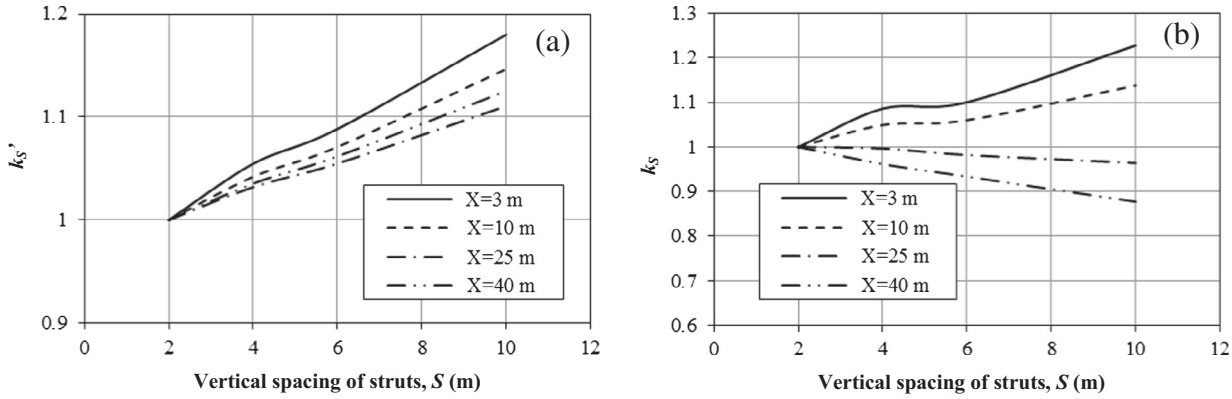

Fig. 17. Influence factors for vertical spacing of struts corresponding to (a) deflection and (b) bending moment.

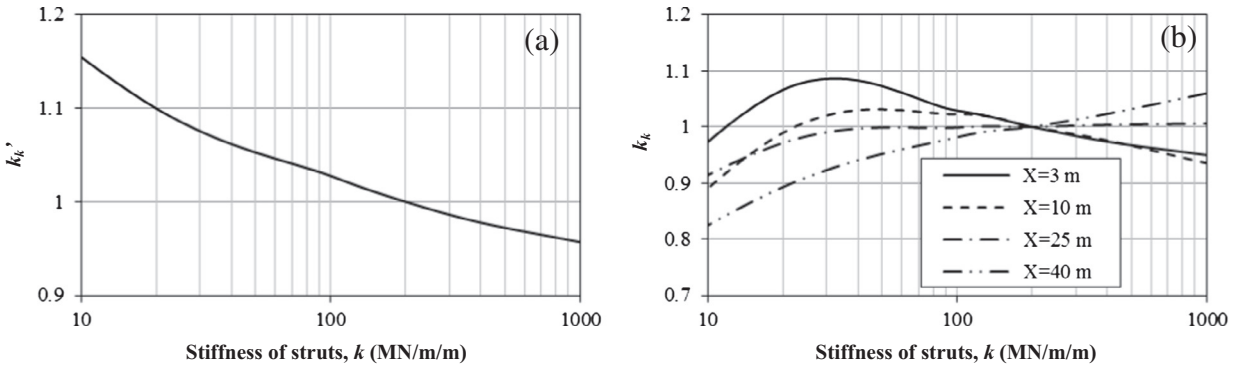

Fig. 18. Influence factors for stiffness of struts corresponding to (a) deflection and (b) bending moment.

bending moment and pile lateral deformation are calculated from the design charts for excavation depths of 4, 8, 12, 16 and 20 m. In addition, a three-dimensional finite element analysis is carried out for the same problem to compare with the predictions from the design charts.

Step 1: The maximum lateral deformation and bending moment for the base case using Eqs. (2) and (3) at $X = 25$ m are: $d_b = (H/100)e^{-0.375}$ m and $M_b = 140He^{-1.25}$ kN m. Next, influence factors needs to be obtained from Figs. 15–19.

Step 2: The undrained shear strength, c_u, is calculated using Eq. (4). Since c_u varies along the depth, average c_u over the depth of excavation was obtained for each excavation stage of the analysis using Fig. 15(a) and (b), $k'_{cu} = 1.23, 1.15, 1.05, 0.94, 0.8$ and $k_{cu} = 1.0, 1.11, 1.03, 0.93, 0.9$ for the excavation depths of 4, 8, 12, 16 and 20 m.

Step 3: The diameter of the pile is 1.5 m. Hence, based on Fig. 16 (a) and (b), $k'_d = 0.98$ and $k_d = 3.75$.

Step 4: Based on Fig. 17(a) and (b), for a strut spacing of 4 m, $k'_s = 1.02$ and $k_s = 1.0$.

Step 5: The stiffness of the struts used for the wall support system is 100 MN/m/m. Therefore, from Fig. 18(a) and (b), $k'_k = 1.03$ and $k_k = 1.0$.

Step 6: The unsupported depth of the wall is 2 m. Hence from Fig. 19(a) and (b), $k'_{h_{un}} = 1.1$ and $k_{h_{un}} = 0.83$.

Fig. 20(a) and (b) shows the maximum pile lateral deformations and bending moments, respectively, from the finite element anal-

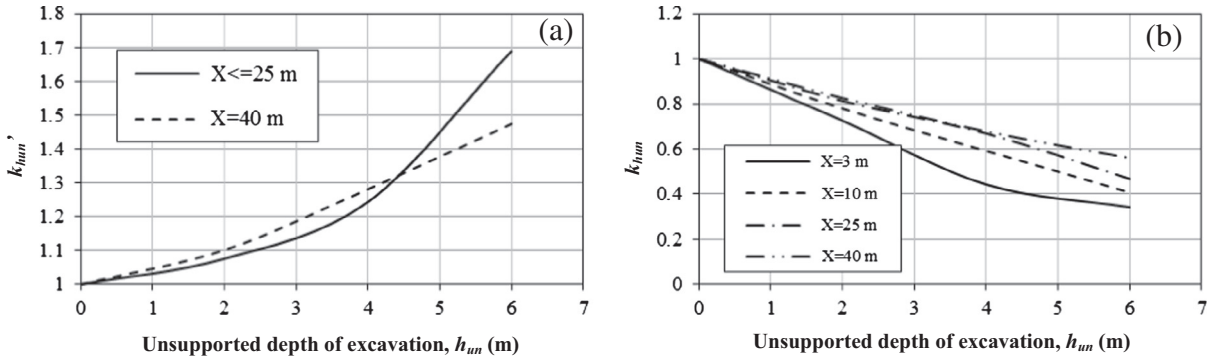

Fig. 19. Influence factors for unsupported depth of excavation corresponding to (a) deflection and (b) bending moment.

ysis and the design charts. These results show that the proposed design charts are useful for practicing geotechnical engineers to assess the influence of nearby excavations on existing nearby pile foundations.

5.2. Comparison of results with measured data from a case study and simplified design charts by Poulos and Chen (1997)

In this section, the results from the design charts will be compared with the case study reported by Finno et al. (1991) and the predictions for the same case study by Poulos and Chen (1997) based on the design charts proposed by them. The case study is about the performance of groups of step-tapered piles adjacent to a 15.4 m deep excavation. The excavation is carried out within an existing framed structure, where the main columns are supported by concrete piles. The ground profile consists of 9.14 m of sandy fill, 7.62 m of clay and below that there is another alluvial sand deposit. The SPT N values for the site before and after the excavation are available to derive soil properties. The wall is supported by tie backs. According to Poulos and Chen (1997), they are equivalent to four levels of supports whose stiffness is equivalent to 1×10^4 kN/m/m placed at a spacing of 5 m. The average unit weight of the soil is 19 kN/m^3. The closest piles to the excavation are 1.5 m from the face of the excavation. The step-tapered piles used in the case study has an equivalent diameter of 327 mm and a length of 25 m.

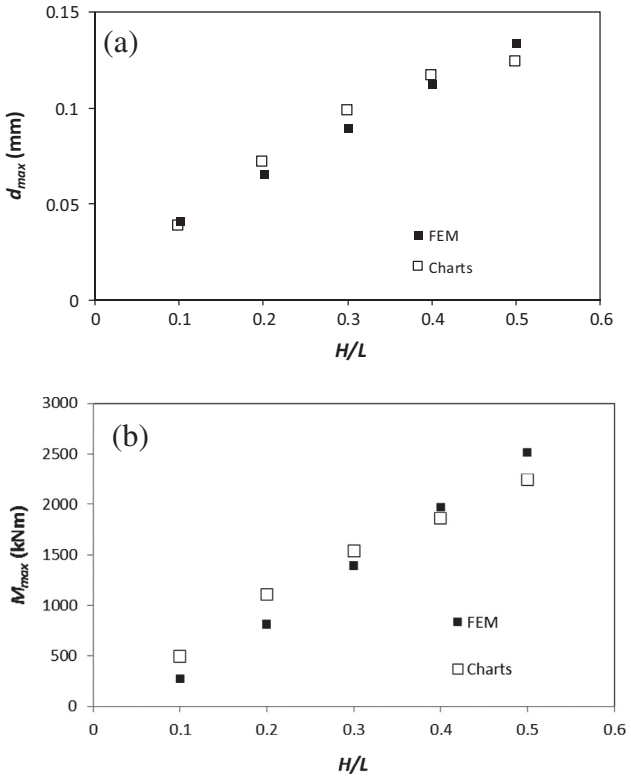

Fig. 20. Comparisons of (a) lateral deformation and (b) bending moment obtained from finite element analysis and charts.

According to Finno et al. (1991), the maximum pile lateral deformations recorded at the site after excavation depths of 6.71 m and 15.24 m are 38 mm and 63 mm. Poulos and Chen (1997) also simulated the same excavation using a two-step analysis procedure. In the first step, a plane strain finite element analysis is carried out to obtain the free field ground deformations without the pile and then the free field ground deformations are used to obtain the pile behaviour in the second stage of the analysis. Pile lateral deformations predicted from the two-step finite element analysis was identical to the above mentioned field measurements. The bending moments developed in piles were not measured in the case study but Finno et al. (1991) and Poulos and Chen (1997) predicted them using finite element analyses. The maximum pile bending moments predicted by Finno et al. after 6.71 m and 15.24 m excavation depths are 19 kN m and 16 kN m, respectively. Poulos and Chen predicted bending moments of 15 kN m and 25 kN m after 6.71 m and 15.24 m excavation depths, respectively.

Using the above data for the case study, design charts proposed in this paper are used to calculate the maximum pile lateral deformation and the bending moment. In this case, we need c_u to obtain the influence factors k'_{c_u} and k_{c_u}. As mentioned in Section 5.1, the average c_u should be computed over the depth of the excavation for each excavation stage. In this case, the top layer is sand and the 6.71 m excavation is carried out within the 9.14 m deep sand layer. Hence an equivalent c_u was obtained considering the post excavation average SPT N values over the sand layer, which is 10. SPT $N = 10$ corresponds to a c_u of 128.6 kPa, based on the chart given by Terzaghi and Peck (1967). For the 15.24 m excavation, c_u was calculated as a weighted average over the excavation depth because base of the excavation lies 6.1 m into the clay layer below the sandy fill. For the clay layer average SPT N is 20 and hence c_u is 266.7 kPa according to Terzaghi and Peck (1967), which gives a weighted average c_u of 157 kPa over the excavation depth of 15.24 m. To obtain the maximum pile deformation and bending moment, following calculation steps were performed:

Step 1: The maximum lateral deformation and bending moment for the base case computed using Eqs. (2) and (3) at $X = 1.5$ m are: $d_b = (H/100)e^{-0.015\times1.5}$ m and $M_b = 140He^{-0.05\times1.5}$ kN m.

For $H = 6.71$ m, $d_b = 65.6$ mm and $M_b = 871.5$ kN m. For $H = 15.2$ m, $d_b = 149.0$ mm and $M_b = 1979.4$ kN m. Next, the influence factors needs to be obtained from Figs. 15–19.

Step 2: The undrained shear strength, c_u, for the $H = 6.71$ m is 129 kPa and for $H = 15.2$ m is 157 kPa. The influence factors for the two excavation stages are respectively, $k'_{cu} = 0.56, 0.31$ and $k_{cu} = 0.63, 0.41$ based on Fig. 15(a) and (b).

Step 3: The diameter of the pile is 0.327 m. Hence, based on Fig. 16(a) and (b), $k'_d = 1.04$ and $k_d = 0.03$.

Step 4: Based on Fig. 17(a) and (b), for a strut spacing of 5 m, $k'_s = 1.1$ and $k_s = 1.1$.

Step 5: The stiffness of the struts used for the wall support system is 1×10^4 kN/m/m. Therefore, from Fig. 18(a) and (b), $k'_k = 0.96$ and $k_k = 0.95$.

Step 6: The unsupported depth of the wall is 0 m. Hence from Fig. 19(a) and (b), $k'_{h_{un}} = 1.0$ and $k_{h_{un}} = 1.0$.

If the maximum pile lateral deformation and bending moment for the base case, and the influence factors given in the above steps are substituted in Eqs. 5(a) and 5(b), maximum lateral pile deflections of **41 mm** and **51 mm**, and maximum pile bending moments of **17 kN m** and **26 kN m** are obtained for the $H = 6.71$ m and $H = 15.2$ m, respectively.

According to the design charts proposed by Poulos and Chen (1997), the maximum lateral pile deflections of 26 mm and 52 mm, and maximum pile bending moments of 13 kN m and 25 kN m are obtained for the $H = 6.71$ m and $H = 15.2$ m, respectively. These results clearly show that the maximum pile lateral deformations obtained from the proposed design charts agree well with the field measurements (38 mm and 63 mm) at both excavation depths. Bending moments were not measured in the field but the design charts produced maximum pile bending moments in agreement with the two-dimensional finite element analysis results (15 kN m and 25 kN m) given by Poulos and Chen (1997). Although design charts produced by Poulos and Chen (1997) are based on an undrained analysis with two separate steps to obtain ground deformations and then the pile response using those ground deformations, results obtained from their design charts are also in close agreement with the results from this study apart from the pile lateral deformation after the first excavation stage.

6. Conclusions

This paper investigated single pile behaviour due to ground deformations caused by deep excavations using a three-dimensional finite element model, which has been verified using centrifuge test data found in the literature. A detailed parametric study is carried out investigating the influence of excavation depth, pile location with respect to the wall, stiffness and spacing of the wall support system, overconsolidation ratio of the soil and pile head fixity condition. Results show that pile lateral deformation and bending moment increases significantly with excavation depth. For a particular excavation depth, the maximum lateral deformation and bending moment of the pile decay exponentially with the distance from the excavation. The influence of stress history on pile behaviour is observed varying overconsolidation ratio of the soil. With increasing overconsolidation ratio, both pile lateral deformation and maximum bending moment decrease. When struts are installed closely, maximum lateral deformation occurs well below the excavation depth. However, with increasing strut spacing, the location of the maximum pile bending moment moves towards the base of the excavation. When the stiffness of the struts exceeds 10 MN/m/m, support system does not have a significant influence on pile behaviour but when it decreases below 10 MN/m/m, maximum pile bending moment and lateral deformation increases.

Pile head fixity has a huge impact on the development of bending moments along the pile. With increasing degree of pile head fixity, the development of negative bending moment near pile cap is very high. If additional bending moments are developed in piles due to nearby excavations, axial load carrying capacity of piles decreases significantly. Hence, it is important to assess how the induced bending moments will affect the structural capacity of pile foundations, when an excavation is planned to be carried out near an existing loaded pile.

Finally, a set of design charts are derived using the results from the parametric study. These charts are useful in predicting maximum pile lateral deformation and bending moment during a nearby excavation but valid only for piles founded in clayey soils, within 40 m from the excavation face. The capability of the proposed design charts are demonstrated using a three-dimensional finite element analysis, a case study and a simplified prediction method based on the design charts from the literature. Results show that these charts are useful in predicting maximum pile deformation and bending moment due to nearby excavations at the preliminary stage of a design project to ascertain the ability of nearby piles to carry excavation induced ground movements.

Acknowledgement

The authors would like to acknowledge the financial assistance provided by the Australian Research Council, Australia for this research under the Discovery Grant DP1094309.

References

ABAQUS/Standard, 2011. ABAQUS version 6.11 user's manual, Providence, Rhode Island, USA.

Broms, B., 1979. Negative skin friction. In: Proceedings, 6th Asian Regional Conference, Soil mechanics and Foundation Engineering, Singapore, pp. 41–75.

Brown, D.A., Shie, C.F., 1990. Three dimensional finite element model of laterally loaded piles. Comput. Geotech. 10, 59–79.

Chen, L.T., Poulos, H.G., 1996. Some aspects of pile response near an excavation. In: Proceedings, 7th Australia New Zealand Conference on Geomechanics: Geomechanics in a Changing World, Barton, ACT: Institution of Engineers, Australia, pp. 604–609.

Finno, R.J., Lawrence, S.A., Harahap, I.S., 1991. Analysis of performance of pile groups adjacent to deep excavation. J. Geotech. Geoenviron. Eng. 117 (6), 934–955.

Goh, A.T.C., Wong, K.S., Teh, C.I., Wen, D., 2003. Pile response adjacent to braced excavation. J. Geotech. Geoenviron. Eng. 129 (4), 383–386.

Guo, W.D., Ghee, E.H., 2006. Behavior of axially loaded pile groups subjected to lateral soil movement. In: Foundation Analysis and Design, Innovative Methods, Proceedings of Sessions of GeoShanghai, Shanghai, China, pp. 174–181.

Hashash, Y.M., Whittle, A.J., 1996. Ground movement prediction for deep excavations in soft clay. J. Geotech. Eng., ASCE 122 (6), 474–486.

Leung, C.F., Chow, Y.K., Shen, R.F., 2000. Behaviour of pile subject to excavation-induced soil movement. J. Geotech. Geoenviron. Eng. 126 (11), 947–954.

Miao, L.F., Goh, A.T.C., Wong, K.S., Teh, C.I., 2006. Three-dimensional finite element analyses of passive pile behaviour. Int. J. Numer. Anal. Methods Geomech. 30 (7), 599–613.

Nishanthan, R., Liyanapathirana, D.S., Leo, C., 2014. Modelling issues in simulation of deep excavations. Aust. Geomech. J. 49 (1), 91–103.

O'Rouke, T.D., 1981. Ground movements caused by braced excavation. J. Geotech. Geoenviron. Eng. 107 (9), 1159–1178.

Ong, D.E.L., Leung, C.E., Chow, Y.K., 2006. Pile behaviour due to excavation-induced soil movement in clay I: Stable wall. J. Geotech. Geoenviron. Eng. 132 (1), 36–44.

Park, R., Paulay, T., 1975. Reinforced Concrete Structures. John Wiley, New York.

Potts, D.M., Zdravkovic, L., 2001. Finite element analysis in geotechnical Engineering. Thomas Telford, London.

Poulos, H.G., Chen, L.T., 1996. Pile response due to unsupported excavation-induced lateral soil movement. Can. Geotech. J. 33 (4), 670–677.

Poulos, H.G., Chen, L.T., 1997. Pile response due to excavation-induced lateral soil movement. J. Geotech. Geoenviron. Eng. 123 (2), 94–99.

Poulos, H.G., 2005. The influence of construction side effects on existing pile foundations. Geotech. Eng. 36 (1), 51–67.

Sagaseta, C., 1987. Analysis of undrained soil deformation due to ground loss. Geotechnique 37 (3), 301–320.

Teh, K.L., Leung, C.F., Chow, Y.K., 2005. Spudcan penetration in sand overlying clay. In: Gourvenec, Cassidy (Eds.), Proceedings of Frontiers in Offshore Geotechnics: ISFOG 2005, Perth, Australia, pp. 529–534.

Terzaghi, K., Peck, R.B., 1967. Soil Mechanics in Engineering Practice. John Wiley, NewYork.

Wroth, C.P., Houlsby, G.T., 1985. Property characterization and analysis procedures. In: Proceedings of the 11th International Conference of Soil Mechanics and Foundation Engineering, San Francisco, vol. 1, pp. 1–55.

Xu, K.J., Poulos, H.G., 2000. Theoretical study of pile behaviour induced by a soil cut. In: Proceedings of GeoEngineering 2000, Melbourne.

Zhang, R., Zheng, J., Pu, H., Zhang, L., 2011. Analysis of excavation-induced responses of loaded pile foundations considering unloading effect. Tunnelling Underground Space Technol. 26 (2), 320–335.